Article:

Rashid, F, Glover, PWJ orcid.org/0000-0003-1715-5474, Lorinczi, P et al. (2 more authors) (2017) Microstructural controls on reservoir quality in tight oil carbonate reservoir rocks. Journal of Petroleum Science and Engineering, 156. pp. 814-826. ISSN 0920-4105

https://doi.org/10.1016/j.petrol.2017.06.056

Microstructural controls on reservoir quality in tight oil carbonate reservoir rocks

Rashid, F.[1], Glover, P.W.J.[2], Lorinczi, P.[2], Hussein, D.[3], Lawrence, J. A[4].

1- Oil, Gas and Energy Management Department, CANM, Charmo University, Iraq. Email:fraidoon.rashid@charmouniversity.org, Phone: +9647701924416
2- School of Earth and Environment, University of Leeds, UK
3- Geology Department, University of Sulaimani, Iraq.
4- Department of Civil and Environmental Engineering, Imperial College London, UK.

Abstract

In carbonate reservoir rocks the complex interaction between the petrophysical properties corresponds to the various depositional microstructures which are modified by various diagenetic processes that ultimately define the reservoir quality, and pose challenges to the prediction of permeability. The permeability heterogeneity in the carbonate oil reservoirs of northern Iraq varies widely and is thought to be controlled by a number of different factors. In this work, controls of matrix permeability for the Cretaceous Kometan formation selected from five oil fields in Kirkuk embayment zone have been investigated. Helium porosity, helium pulse decay permeability , brine permeability, Nuclear Magnetic Resonance (NMR), Mercury Injection Capillary pressure (MICP) , Scanning Electronic Microscopy (SEM), X-Ray diffraction (XRD), and photomicrography of thin section have been used to investigate the effect of microstructure on the variation of permeability in the Kometan Formation. The formation has porosities and permeabilities which range from 0.5±0.5% to 29±0.5% and from 0.65±0.08 μD to 700±0.08 μD respectively. Three types of pore systems have been investigated using pore type, pore size and pore-throat size as characterizing parameters. We have recognized three microstructural types: (i) matrix composed of nano-intercrystalline pores (pore diameter d_p smaller than 1 μm and a nanoporous pore-throat size), (ii) matrix composed of micro-intercrystalline pores ($1<d_p<10$ μm with a corresponding micron-scale pore-throat distribution), and (iii) meso-intragranular and moldic pores ($d_p>10$ μm) also with microporous pore-throat radii. The nano-intercrystalline pore system is common across northern Iraq and represents the effective pore system type in the reservoirs of the Kirkuk embayment zone. For these

tight carbonate reservoirs, the mineralogy, especially of quartz and clay minerals (illite and smectite), has little relationship with the measured Klinkenberg-corrected permeability. Consequently, mineralogy is not a useful controlling factor for permeability. Diagenetic processes have altered the depositional texture significantly, resulting in changes to the pore size and pore-throat size distribution and affecting the permeability. In addition the matrix permeability is sensitive to stress, with permeability decreases between -4×10^{-4} mD/psi and -4×10^{-5} mD/psi in the effective stress range from 0 psi to 4000 psi. It has been found that of the three microstructure pore types the nano-intercrystalline pore system is more sensitive to increasing effective stress compared to the micro-intercrystalline and meso-intragranular pore systems. Laboratory experiments have shown that stylolisation resulting from regional fluid movements has also affected matrix permeability, with the stylolites acting as barriers to fluid flow and considered to be an important source of tightness of the Kometan formation in the Kirkuk embayment fields.

1. Introduction

Many carbonate rocks are complex and heterogeneous over a large scale range due to the intercalation of varied depositional textures and post-depositional diagenetic modification of original rock. The result is a rock of variable reservoir quality, which is a challenge to evaluate, especially if the goal is to predict reservoir permeability (Ehrenberg and Nadeau, 2005; Ehrenberg, 2006, Lucia, 2007; Harris, 2010; Palermo et al., 2010; Ronchi et al., 2010; Rashid et al., 2015a). There are many factors governing the petrophysical properties of carbonates which are essential if conceptual and numerical reservoir models are to be constructed (Briguad et al, 2010).

The prediction of most petrophysical properties in carbonate reservoir rocks is problematic. This is especially true of permeability and fluid flow because the carbonate rocks often have heterogeneous grain sizes. Those grain sizes are not related simply to pore and pore-throat neither dimensions nor are they just related to the connectivity of pores, as represented by the cementation exponent m. But they can vary laterally and with depth both at large scales and often changing significantly over small distances as well (Rashid et al., 2015a). This variability is the result of tectonic deformation and diagenesis that has continuously altered the parent reservoir rock properties (Wilson and Evans, 2002; Westphal et al., 2004; Davis et al., 2006; Dou et al., 2011; Rong et al., 2012; Rashid et al., 2015b). The combination of these factors controls the microstructure of the pore system and ultimately dictates the distribution of permeability in the carbonate rocks, and hence affects reservoir potential and individual well productivity (Chalmers, 2012; Haines et al., 2016).

Accordingly, prediction and evaluation of the permeability of a carbonate reservoir implies an investigation of the properties of its pore microstructure (Anselmetti and Eberli, 1999; Budd, 2002; Melim et al., 2001; van der Land et al., 2013). Budd (2002) has quantified pore system modifications by integrating cementation and compaction in carbonate grainstones with the aim of evaluating permeability. More recently, Makhloufi et al. (2013) investigated the variation of petrophysical parameters associated with sedimentological and diagenetic changes in tight oolitic limestone, while Haines et al. (2015) documented the evolution of pore systems corresponding to fault damage and the associated diagenesis in carbonate lithologies.

The objective of this paper is to characterise the pore system modifications which arise from textural changes in tight carbonate reservoir rocks in the Kirkuk embayment fields, and then to consider the combined effect of these textural modifications on the value and variability of matrix permeability. The second part of this work considers both the sensitivity of the permeability of reservoir rocks to changes in effective stress through its effect on the pore microstructure, as well as the effect of stylolitisation and its control on the spatial and temporal evolution of permeability in unconventional tight carbonate rocks. These results can be applied to subsurface reservoirs to improve reservoir quality predictions especially in the newly discovered oil fields and licensed blocks throughout the region.

2. Sampling and methods

2.1 Sample provenance

This study characterises the pore system modifications which arise from textural changes in tight carbonate reservoir rocks in the Zagros Folded belt oil fields, and then considers their combined effect on matrix permeability and its variability. The second part of this work considers both the sensitivity of the permeability of reservoir rocks to changes in effective stress through its effect on the pore microstructure, as well as the effect of stylolitisation and its control on the spatial and temporal evolution of permeability in unconventional tight carbonate rocks. These results can be applied to subsurface reservoirs to improve reservoir quality predictions especially in tight carbonate reservoirs.

The Zagros Folded Belt covers the northern part and Kurdistan region of Iraq, and is characterized by the extension of several NE-SW trending structures. The data analysed in this work, including outcrop studies, samples, well cores and logs, were gathered primarily from five oil fields including the Taq Taq, Kirkuk, Jambur, Khabaz and Bai Hassan oil fields (Figure 1). The Kometan Formation is primarily composed of two beds; a globogerinal limestone (K_1) and a mixed globogerinal/oligostiginal limestone (K_2), commonly separated by a glauconitic limestone bed, and a shaly limestone unit which occurs throughout the western part of the zone, especially in the Khabaz and Bai Hassan oil fields (Figure 2). Throughout most of the Zagros Folded and Thrust belt, the limestone beds of the Kometan Formation are highly stylolitic, compacted, thin and homogenous, while they become non-stylolitic, massive limestone beds towards the western margin of the Zagros Folded belt fields (Figure 1). The limestone beds of the Kometan Formation are classified as tight carbonate reservoirs (Rashid et al., 2015a). Their porosity ranges between 0.5±0.5% to 29±0.5%, and have permeabilities ranging from 0.65±0.08 μD to 700±0.08 μD. The porosity values in the majority of the studied area do not exceed 10±0.5% with the exception of the Bai Hassan and Khabaz fields, where the porosity increases to 29±0.5%.

The material collected for analysis in this study included 205 core plug samples representing 99 m of core from one well in each of the 5 fields, as specified in Table 1.

Sampling was not necessarily representative of the whole thickness of the formation. The positions of samples were selected based on apparent oil saturation, stylolite distribution, the presence of fractures and lithological variation. All core plugs were nominally 1.5 inches in diameter and 2 inches long. The research materials are summarised in Table 1.

Table 1. Core sampling and testing strategy

Location	Well	Core Length (m)	Core plug numbers	Core measurements number for each analysis type							
				He Porosity	He Permeability (mD)	Brine Permeability (□D)	SEM	XRD	Thin section	NMR	MICP
Taq Taq Field	Tq-1	18	50	50	50	4	2	5	3	10	2
Kirkuk field	K-243	18	61	61	61	4	6	3	4	7	7
Jambur field	J-37	18	19	19	19	2	3	7	7	10	3
Bai Hassan field	BH-13	36	55	55	55	3	9	4	6	15	9
Khabaz field	Kz-13	9	20	20	20	2	2	4	2	2	2

2.2 Mineralogy

Subsets of 23 samples were selected based on physical appearance, textural change, pore system modifications and gamma ray reflection of the studied intervals. The samples were roughly broken up with a hammer, before being mechanically crushed with a pestle in an agate mortar until they formed powder. A McCrone micronising mill was then used to produce a material with a more uniform grain size, typically 8 μm diameter according to manufacturer's specification after a 12 minute grind. The XRD analysis was carried out on a Philips PW1050 using Cu-K alpha radiation and fitted with a secondary Graphite monochromator. The scan parameter was 3-70 Deg 2 theta, step size of 0.01^{o} and a speed of 0.6^{o}/min.

2.3 Image analysis

22 thin sections, impregnated with Methylene blue dyed epoxy resin, and alizarin red were used to determine the texture, grain type and pore-type distribution. The samples were obtained depending on porosity and permeability relationship and rock texture distribution throughout the studied samples. Thin section photomicrography did not provide effective results for the identification of pore types. Pore types in the sample material were visualized by using high-resolution HRFE-SEM (High resolution field emission scanning electron microscope) with magnifications of 1:10,000 and 1:20,000. A total of 22 samples, 70 mm in size, and with broken surfaces were glued on to aluminium stubs for imaging. The sample material was cleaned using 1% acetic acid solvents to remove any dust or volatile hydrocarbons that may have affected the result, before being coated with a conducting carbon film prior to digital recording of the SEM images.

The recorded images were analysed using ImageJ software (thresholding technique). Pore sizes were measured using Feret's diameter (Ferreira and Rasband, 2012). Multiple measurements of pore sizes were taken for each identified pore on each image. The number of pore size measurement was varied with the amount of pores appeared on each SEM image. An arithmetic mean pore diameter together with a measure of measurement variability was recorded for each sample.

2.4 Porosity and permeability

A helium gas expansion porosimeter (pycnometer) was used to quantify Helium porosity on the 205 core plugs corresponding to the 99 m of available rock samples. The core plugs were 1.5 inch (38 mm) in diameter and 2.0 inches (51 mm) in length. The estimated porosity can be made to within ±0.1 porosity unit using the apparatus and protocols at the University of Leeds.

The permeability of cored plug samples was measured using a helium pulse-decay permeameter. This technique works by monitoring the decay of the fluid pressure which is caused by fluid leaking through the sample (Jannot et al., 2007; Zhang et al., 2000; Jones, 1997; Dicker and Smits, 1988; Bourbie and Walls, 1982; Amaefule et al., 1986). Samples were tested at an effective stresses of 800 psi and at four pore fluid pressures (100,150, 200 and 250 psi respectively) in order to calculate the Klinkenberg-corrected permeability for each sample throughout the study area Helium gas . In addition, brine was used for measuring permeability to selected samples for understanding the influence of mineralogy on permeability variation. The composition of the brine was derived from the formation water collected from the studied reservoir in the northern Iraq oil fields as shown on Table (2), (NOC,1987).

To understand the variation of permeability as a function of effective stress, the Klinkenberg-corrected He gas pulse decay permeability was also measured for 9 different effective stress points with confining pressure of 0 to 4000 psi. This procedure was carried out for a subset of 6 samples as it is very time-consuming. The samples were chosen on the basis of their texture, porosity, permeability, pore size, pore throat size and pore types.

The influence of stylolisation on permeability variation throughout tight carbonate rocks was examined in this study. Two sub-sets of stylolitic and non-stylolitic samples of the same well interval and rock textures were selected for permeability measurement. The gas flow movement in this experiment was perpendicular and parallel to the surface of the stylolite's (90° and 0°) using Pulse Decay technique and klinkenberg corrected permeability measurements.

Table 2. Brine composition used in this study, (NOC, 1987).

Component	Amount (g/l)
$NaCO_2$	0.00521
$CaCO_2$	0.00077
$MgCO_2$	0.00023
NaS_2	0.0079
NaCl	0.01489
Equivalent NaCl	0.03695

2.5 Mercury Injection capillary pressure (MICP)

The mercury injection capillary pressure (MICP) applies pressure up to 60000 psi to calculate pore-throat diameter distribution of the measured sample. The intrusion data were collected using a Micromeritics Autopore IV 9250 apparatus (Giesche, 2006) for 23 samples in this study. Pore system and rock texture distributions were considered for sample selection. The mercury was injected using 62 pressure steps that were distributed logarithmically, and pore-throat size distributions were calculated using the Washburn equation in the usual way (Washburn, 1921; Webb, 2001).

A pore-throat size corresponding to the threshold pressure point on the capillary pressure curve was used as an effective pore throat size that provides a connected pathway to fluid flow through the tight carbonate reservoir samples (Katz and Thompson, 1987). This value can be used as a convenient parameter for permeability prediction (Rashid et al., 2015b).

2.6 Nuclear Magnetic Resonance (NMR) spectroscopy

The NMR measurements were taken using a Resonance Instruments MARAN 2 bench top spectrometer at atmospheric pressure, 25 ℃ and 2 MHz. The relaxation time distribution was measured using the MARAN 2 DXP program for 44 samples. Some experimental data about pore size distribution can be obtained from the magnetization modification of water molecules that fill the pore spaces of the analysed samples. The relaxation time T_2, which is the time of transverse magnetization decay, was measured on each sample. The samples were first saturated with formation water at 1000 psi confining pressure for 24 hours at room temperature in order to fill all their pores with brine, and then the saturated samples were placed in a glass tube which was inserted into the NMR system.

NMR signals were obtained from the brine when the sample was located in a magnetic field and then excited with a brief pulse of radio frequency energy (Coates et al., 1999). The relaxation time (T_2) provides an efficient signal corresponding to the pore size distribution in porous media. Large pores have longer T_2 values than smaller pores (Westphal et al., 2005; Heath et al., 2011; Al Hinai et al., 2014).

3. Results

3.1. Mineralogy

All samples were predominantly limestone with clay content below 4% except for 2 samples which were gathered from the shaly limestone unit, and which have a mean clay content of 49%. The calcium carbonate content of all samples was correspondingly high, usually ≥ 92% throughout the study area, this value reduced to 45% in the shaly limestone samples. Quartz content averaged at about 2% and ranges between zero and 4.5%. Illite and smectite dominate the clay content with an average of 1.1 % and ranges between zero and 3.7% without any recording of chlorite and kaolinite clay minerals. Dolomite was identified in some samples taken from Bai Hassan and Khabaz fields. In these fields, a dolomite mineral averages 1.1% with a range between zero and 11%. Pyrite was only observed in one shaly limestone sample (1.1%).

3.2 Pore system

In this sub-section we describe the pore type, pore size and pore-throat size of the measured samples. Pore types were classified from image analysis based on porosity classification systems of Choquette and Pray (1970). Pore types were subdivided into three classes, derived from depositional and diagenetic modification of rock textural characteristics. The pore types included intercrystalline, moldic and intergranular pores.

Pore sizes were sub grouped into three classes: nano-, micro-, and meso-pore sizes. The nano-pore size class includes all pores with a diameter of less than 1 µm. The micro-pore size class includes all pores with a diameter between 1 µm and 10 µm, and the meso-pore size class includes all pores with a diameter greater than 10 µm, and reaching as high as 200 µm. The pore sizes were measured using ImageJ for 22 samples, and longitudinal relaxation time distributions (T_2) for 44 samples. The measured pore diameters were used to calibrate the T_2 measurements with the nano-pores having diameters smaller than 1 µm and being associated with short relaxation times, smaller than 100 ms, while micro-pores provided T_2 values greater than 100 ms, and very high relaxation times being observed for moldic and intragranular pores, generally greater than 200 ms. The classification of Porras and Campos (2001) was used to characterise pore-throat sizes derived from MICP analyses with micro-porous textures having pore-throat radii between 0.5 and 0.2 µm, and nano-porous textures being associated with pore-throat radii smaller than 0.2 µm.

Three types of pore systems were recognised throughout the studied area, classified by their pore type, pore size and pore-throat size ranges. These are defined in Table 3 and presented in Figure 3. Nano-intercrystalline represents the most common type of pore system throughout the studied samples, covering 80% of the analysis samples. It is characterized by intercrystalline pore types that have nano-scale pore diameter and nano-porous pore throat size. Consequently, 14% of the measured samples referred to the micro-intercrystalline pore system. This pore system is identified from micro-pore size intercrystalline pores that are interconnected by micro-porous pore throat size. Meso-intragranular and moldic pore systems are considered the third type of observed pore system and extended to about 6% of the collected samples. Pore types were dominantly recorded as intragranular and moldic pores with meso-pore size and micro-porous pore throat size.

Table 3. Pore system classifications used in this work.

Pore Systems	Pore Types	Pore Sizes (μm)	Pore-throat sizes (μm)	NMR T_2 (ms)
Nano-intercrystalline	Intercrystalline	< 1	< 0.2	< 100
Micro-intercrystalline	Intercrystalline	1 – 10	0.2 – 0.5	100 – 200
Meso-intragranular/moldic	Intragranular	>10	> 0.5	> 200

Nano intercrystalline pore systems are the dominant type in the reservoir samples studied throughout the oil fields in the Zagros Folded belt.

3.3 Porosity and permeability

Generally, porosity and permeability are positively correlated, and the relationship between them is a power law (Figure 4). This poroperm diagram, which treats the three pore types separately, shows measurements of porosity and permeability for the nano-intercrystalline, micro-intercrystalline and meso-intragranular pore systems respectively.

The overall permeability of the reservoir rock is low with values ranging from 65±0.08 nD to 700 ±0.08μD. The nano-intercrystalline pore system has a porosity ranging from 0.5±0.5% to 10±0.5%, and permeabilities which range from 0.65±0.08 μD - 51±0.08 μD (Figure 4; green shading). In micro-intercrystalline pores, porosity is enhanced by comparison to the nano-intercrystalline pore system, with porosities ranging from 12±0.5% to 25±0.5% and correspondingly larger permeabilities, between 65±0.08 μD to 600±0.08 μD (Figure 4; blue shading). The third pore system type has porosity greater than the two previous pore systems. The measured porosity in the meso-intragranular/moldic pore system ranges from 20±0.5% to 29±0.5%; and the permeability lies between 90±0.08 μD and 700±0.08 μD (Figure 4; red shading). The poroperm statistics for each pore system are presented in Table 4.

Anisotropic permeability was examined by carrying out measurements on horizontal and vertical plugs taken from the core samples using pulse decay technique for measuring Klinkenberg corrected permeability. The sample selection procedure was arranged based on matrix texture, and pore system of the rock samples as well as core sample availability. For the Kometan Formation, fluid flow is isotropic at a core-plug scale, with the horizontal and vertical permeabilities showing similar values (Figure 5). The small differences between the vertical and horizontal permeabilities can be ascribed to heterogeneity of the rock texture and sample selection.

The porosity and permeability distributions throughout the study area correlate dominantly with diagenetic modification of the rock structure, and this variation causes extensive heterogeneity in reservoir quality. The nano-intercrystalline pore system occurs within the globogerinal limestone (K_1) and mixed globogerinal/oligostiginal limestone (K_2) rock units from the majority of the studied fields in the Kirkuk embayment. This type of pore system has poor reservoir quality because cementation, compaction and stylolisation together reduce reservoir potential. In contrast, the dominant pore types in the western part of the Kirkuk embayment fields are the micro-intercrystalline pore system, which is associated with the globogerinal limestone (K_1), and the meso-intragranular pore system, which was recorded in mixed globogerinal/oligostiginal limestone (K_2) only. In this part of the study area the lack of stylolisation and the effect of dissolution has enhanced reservoir quality, especially porosity and permeability, within the reservoir rock units.

Table 4. Poroperm statistics for the three pore systems.

Static parameters	Nano-intercrystalline		Micro-intercrystalline		Meso-intragranular	
	ϕ (-) ±0.005	K (μD) ±0.08	ϕ (-) ±0.005	K (μD) ±0.08	ϕ (-) ±0.005	K (μD) ±0.08
Mean	0.5	7	18	380	23	350
Standard deviation	2	8.9	16	140	3	170
Mode	4	10	19	360	20	310
Median	5	4.1	18	390	22	35
Maximum	10	51	25	600	29	700
Minimum	0.5	0.65	12	65	20	90

3.4 Permeability sensitivity to effective stress

The measured samples were selected based on pore system changes throughout the data set. Two samples were taken for each pore system type and submitted to klinkenberg-corrected helium permeametry for 9 confining pressures with a constant pore fluid pressure p = 100 psi, resulting in data for 9 effective pressures σ_e (Figure 6) spanning the range 0 psi to 4000 psi. The ranges of confining pressures were chosen according to the reservoir depth of the Kometan formation throughout the studied fields.

The measured permeability decreases with increasing effective pressure in all cases. The relationship between the permeability and effective stress is non-linear. We have fitted exponential curves to the data to account for the non-linear behaviour. This is a well-recognised pattern (e.g., Chalmers et al., 2012) and is caused by thin-flat high aspect ratio pores, whatever their size, being more sensitive to closure and closing at lower effective stresses, with rounder, lower aspect ratio pores remaining until relatively high effective stresses are attained (Glover et al., 1997; 2000). The closure of the high aspect ratio pores has a greater effect on measured permeability per unit loss of pore volume because their nature causes them to be more interconnected and their loss reduces the overall permeability by a correspondingly larger amount (Glover et al., 1997; 2000).

The low porosity/low permeability nano-intercrystalline pore type is most sensitive to effective stress, following a relationship of the type $k(\sigma_e) = k(\sigma_e = 0)e^{a\sigma_e}$ (Chalmers et al, 2012), where the decay rate *a* is -4×10^{-4} /psi for Sample 1 and Sample 2. Both samples from the micro-intercrystalline pore type and the two samples from the meso-intragranular pore type also follow the same relationship, but this time with an a-value of about -4×10^{-5} /psi, resulting in a much lower sensitivity to effective stress. The permeability of the nano-intercrystalline pore type decreases by about 400% as the effective stress increases, whilst in the other two pore types it only decreased by about 20%.

3.5 Permeability variation with stylolitization

Approximately 8 stylolitic and 16 non-stylolitic core plug reservoir samples were selected from the Bai Hassan and Khabaz oil fields in order to understand the effect of the stylolitization on the fluid flow in the Kometan throughout the studied area. The burial depth of the Kometan Formation is relatively large, varying from 1400 m to 2700 m. The loss in primary porosity and matrix permeability by compaction is consequently significant. Chemical compaction which is represented by relative abundance of stylolites is very common in the Kometan reservoir rocks throughout the Kirkuk embayment fields.

The limestone beds of the Kometan Formation in the Taq Taq, Kirkuk and Jambur fields are characterized by a great abundance of stylolites. By contrast, the presence of stylolites in the Bai Hassan and Khabaz fields was more limited both in number and distribution. Nevertheless, they all share similar petrophysical properties. Overall, the impact of cementation on the rock fabrics of the Kometan Formation is derived from burial cementation and stylolitization, which exercise a great influence on reservoir quality. There is approximately two orders of magnitude difference between the permeability of samples containing stylolites and those which have no stylolites. Furthermore stylolitic samples also have a matrix pore size which is ten times smaller than comparative non-stylolitic samples, showing that cementation is also occurring away from the stylolite itself. Figure 7 shows the poroperm diagram for 24 samples that were chosen to study the effects of stylolisation. The rock textures of two highlighted samples both have similar mudstone microstructure. Both the stylotised and non-stylotised samples conform to an approximately linear relationship on this log-log diagram. The samples that have not undergone the formation of stylolites have much higher porosities (10% to 29%) and permeabilities (60 µD to 0.5 mD) than those containing stylolites, which have porosities in the range 2% to 9% and permeabilities which are also correspondingly low (3 nD -30µD).

It is clear that the formation of stylolites has reduced any reservoir quality that may have been originally present in the rock, not only because of the formation of the stylolite itself, but due also to associated cementation that reduces the pore size significantly.

4. Discussion

4.1. Mineralogy

None of the XRD-analyzed samples showed clay volume compositions in excess of 4% and 0% clay volume were recorded in some samples (Table 1). If one considers all of the samples then those with the highest and lowest permeabilities contain very similar clay volume compositions. Consequently, it would be reasonable to infer that clay volume composition in the Kometan Formation has no significant effect on permeability.

Smectite and illite are the only clay minerals recorded from the XRD analyses. In larger quantities most studies have shown that these clay minerals reduce (Zhao et al., 2016; Chalmers et al., 2012). In this study, we have not observed any clear relationship between permeability and clay content. Furthermore, we have used brine to measure liquid permeability for selected samples in order to understand impaction of clay contents on permeability and accuracy of measured klinkenberg-corrected helium permeability of the same set of samples, but we have not observed any reaction between the brine and mineralogical composition of the rock samples and changing in the magnitude of brine permeability that possibly happen because of rock-water interaction.

All parts of Figure 8 indicate that while mineralogical changes may have some small control on permeability, there are much stronger influences exercised by the initial depositional texture and diagenetic processes which alter the microstructure of the rock but not its mineralogy.

4.2 Initial depositional texture and diagenesis

The initial depositional texture can exercise an important control on the initial pore system, defining the porosity and permeability of carbonate rocks (Loucks, 2002; Lucia, 1995). The original grainstone texture, characterized by highly interconnected inter-particle macro-pores, has permeability much greater than in packstones and wackstones, which mainly contain micro-pores, together with rarer macro-pores and lime mud. In this study we have not observed any micro- and macro-pores in the globigerinal and oligosteginal wackstone and packstone textures because a range of diagenetic and deformational processes has modified the initial depositional texture. These strong diagenetic influences exercise the dominant control on porosity and permeability. They include compaction (Schmoker and Halley, 1982), consolidation (Rashid et al, 2015 a), stylolitisation (Nelson, 1981; Finkel and Wilkinson, 1990), and cementation (Hollis et al., 2010), which all tend to reduce reservoir porosity and particularly permeability, whilst dissolution (Moore and Druckman, 1981; Ahr and Hull, 1983) and dolomitisation can enhance porosity and fluid flow pathways (Al-Qayim and Rashid, 2012). Dissolution, however, often increases porosity with no gross change in permeability because the additional porosity is in the form of isolated pores within a largely unchanged lower permeability matrix. For example, dissolved mudstones have greater magnitude of permeability in comparison with cemented wackstones (Figure 4).

Hence, the reservoir quality of tight carbonates may be controlled to a small amount by its mineralogy, but the primary control is via the microstructure of the pore system and that is defined by the depositional texture and, importantly, by post-depositional diagenetic processes.

4.3. Pore systems

Post-depositional diagenetic textural modifications affect permeability by changing the porosity and pore systems connectivity (Glover 2009; Glover et al., 2010). The ability of fluid to flow from one part of the pore structure to another, for any given porosity, is critically controlled by pore size and even more by pore-throat size (Melim et al., 2001; Weger et al., 2009). Here we assess the impact of changing pore sizes and pore-throat sizes on permeability as well as integrating the relationships with other geological parameters in order to understand the evolution of permeability across tight carbonate rocks.

It has long been recognised that permeability enhancement in carbonates is controlled by pore size for a given porosity with macro-pore connectivity considered to be the essential factor governing permeability (Melim et al., 2001). In this study, we have not observed any macro-pores within the heterogeneous textures of our samples. By contrast we observe three different pore sizes; nano-pores, micro-pores and meso-pores. The correlation between porosity and permeability in carbonate rocks is commonly poor because of their heterogeneous and complex pore systems (Haines et al., 2016). However, the poroperm relationships of the Kometan Formation samples show a clear positive correlation (R^2 = 0.70) between measured porosity and permeability (Figure 4).

The correlation between the magnitudes of the measured Klinkenberg-corrected permeabilities and pore sizes for the 22 samples for which we made pore size measurements using Feret's diameter method (Ferreira and Rasband, 2012) is presented in Figure 9. Comparing the nano-intercrystalline and micro-intercrystalline samples, it can be seen that an increase of about one order of magnitude in pore diameter is associated with a 2 to 3 order of magnitude increase in permeability. This is approximately compatible with the range of permeability prediction models that were primarily designed for clastic rocks where the permeability scales as the square of the grain size (and hence the pore size and pore-throat size) (Glover et al., 2006 Swanson, 1981, and Van Baaren, 1979). However, the pattern between the micro-intercrystalline and meso-intergranular is different. One would expect a further increase in permeability by perhaps one order of magnitude to be associated with a fourfold increase in pore throat diameter, but instead there is a slight decrease in permeability. This may be caused by the pore diameter measurement being dominated by a few large pores that remain isolated within the matrix, and consequently do not contribute to any increase in permeability. These large pores are associated with the presence of foraminifer moulds (*globigerina* and *oligostegina* chambers). The decrease in permeability that is observed is not explained and could be due to the restricted dataset of only 3 samples.. This unexpected increase in permeability associated with an increase in porosity is a very significant observation in carbonate rocks and underlines the heterogeneous microstructure of carbonates and its complex relationship with permeability and porosity (Rezaee et al., 2007 , Palermo et al., 2010, Makhloufi et al, 2013 , and Rashid et al., 2015a; 2015b).

Unlike conventional carbonate reservoir rocks, tight carbonates are characterized by nanometer scale pore-throat sizes (diameters) that provide poor connectivity. Two pore-throat size classes were investigated throughout this research (Table 3). Figure 10 presents a correlation between the magnitudes of the measured Klinkenberg-corrected permeabilities and pore-throat size, with pore-throat size obtained from the pore diameter corresponding to the threshold pressure point on the capillary pressure curve (Katz and Thompson, 1987).

It is immediately clear that the majority of the data are described well by a relationship where the permeability depends on the square of the pore throat size $k = 2.1979 \times d_{PT}^{2.0071}$. Perhaps this should not be surprising as the SI units for permeability are length squared. In fact, there are many equations for the prediction of permeability in clastic rocks which include the length squared term. A review of many of them can be found in either Glover et al. (2006) or Rashid et al. (2015b). That we find a squared relationship when comparing permeability as a function of pore throat size, is interesting because not only does it imply that tight carbonate rocks share some of the microstructural physics that we applied to clastic rocks, it also implies that there is some linear relationship between pore throat size, pore size, and grain size in tight carbonates, i.e., $\boldsymbol{d_{PT}} \sim \boldsymbol{d_{Pore}} \sim \boldsymbol{d_{grain}}$.

4.4. Effective stress

Understanding of the sensitivity of permeability to variations in effective stress is considered to be essential in assessing production from a reservoir rock because pore pressure decreases with production rate and results in an increase in effective stress (Chalmers et al., 2012). Consequently, the initial reservoir permeability is controlled by how the rock microstructure is affected by burial depth, but the sensitivity of the reservoir permeability to change as the reservoir is produced and as the effective pressure increases depends on how sensitive the microstructure of the rock is to changes in effective pressure (Byrnes and Keighin, 1993, Byrnes, 1997 and Ghabezloo et al., 2008), and that microstructure sensitivity can be anisotropic and mineralogy-dependent (Chalmers et al., 2012).

While the variability of permeability with effective stress can be direction-dependent, measurements of vertical and horizontal permeability in the Kometan Formation have shown that the hydraulic conductivity of the horizontal and vertical flows is similar (Figure 6). Whatever small differences exist in the magnitude of the vertical and horizontal permeabilities are probably derived from heterogeneity of the rock texture and sample selection. Based on this result we expect the sensitivity of permeability to effective stress to be the same both vertically and horizontally to the bedding. In other words, we expect the vertical and horizontal permeability have the same sensitivity of variation as function of applied stress.

Due to the sensitivity of the nano-intercrystalline pore system samples were of low reservoir quality, this would be exacerbated when trying to produce from this pore system by further reductions in permeability. The main differences in the sensitivity between the nano intercrystalline and the other 2 pore system type's shows that the stress sensitivity of permeability is strongly controlled by the rock microstructure, which is a result of diagenetic modification, especially modifications that alter the pore-throat size. Nano-porous pore throats are dominantly sensitive to applied stress in comparison to micro-porous throats. Thus, permeability of the highly compacted and cemented rock structures (nano-intercrystalline pore system) decreased more than other pore system once stress was applied. This conclusion is derived from the microstructures and pore system anisotropy throughout the reservoir rocks. The Nano-intercrystalline pore system has considerable contrast between grain sizes and pore sizes, the rock matrix have a grain size greater than 200 μm, while pore sizes are smaller than 1.0 μm and pore throat sizes smaller than 0.1 μm. Any increasing of applied stress compresses available spaces between the matrix grains especially when compared with the two other pore systems. The micro-intercrystalline pore system and meso-intragranular pore system average pore systems are 10 μm and 100 μm respectively.

Consequently, the permeability of Kometan reservoirs in the Bai Hassan and Khabaz fields is less likely to be affected be stress sensitivity than of permeability into account, there is less risk associated with Kometan reservoirs in the Bai Hassan and Khabaz fields in comparison with the fields located in the Kirkuk embayment or recently discovered fields and licensed Kurdistan licensed blocks where the Kometan reservoirs are more sensitive to stress changes (Kirkuk (Baba dome), Jambur and Taq Taq fields).

4.4. Stylolisation

The impact of stylolitisation on permeability and regional fluid flow is considered as a crucial point in petroleum exploration. Stylolites and reprecipitation derived from stylolisation have been identified as dominant destructive factors on reservoir quality. The stylolites decrease porosity and permeability of the parent rocks, and have been investigated as a fluid flow barriers in several reservoir rocks (Nelson, 1981; Burgess and Peter, 1985; Koepnick, 1987; Finkel and Wilkinson, 1990; Dutton and Willis, 1998; Alsharhan and Sadd, 2000). By contrast, several researches have concluded that this type of deformation can enhance reservoir potential (Dawson, 1988; Raynaud and Carrio- Schaffhauser, 1992; Van Geet et al., 2000; Gingras et al., 2002; Harris, 2006; Heap et al, 2014).

In this work, we have already recognised that non-stylolite and stylolite samples have very significantly different power law permeability-porosity relationships (Figure 7). We can say with certainty that in the Kometan Formation stylolites act as barriers to fluid flow. In these rocks reprecipitaed calcium carbonate occludes pores and pore throats reducing connectivity considerably. In addition, data from XRD measurements have shown that the volume of $CaCO_3$ in stylolitic samples is greater than that in non-stylolitic samples by 7%, and we ascribe that increase to the additional calcite cementation associated with stylolitisation. Consequently, we consider the tightness of the Kometan reservoir throughout the majority of the Kirkuk embayment and other parts of the Zagros Fold-Thrust belt has resulted from stylolitisation which is regionally distributed.

5. Conclusions

In this study, 205 core plugs samples were collected from the Cretaceous Kometan Formation in hydrocarbon bearing zone throughout the Kirkuk embayment, Zagros Folded Zone and oil fields for petrophysical, petrographical and mineralogical analysis. The relationships between the mineralogy, texture, pore system, stylolitisation and effective stress variation with permeability were examined, leading to the following conclusions.

1. The original rock textures should not be considered as the single important factor controlling the permeability potential in tight carbonate reservoir rocks because diagenetic modification has significantly changed the depositional rock structure. The resulting pore system has often undergone compaction, consolidation, cementation, and stylolitisation reducing porosity and permeability as well as dissolution and dolomitisation which may enhance porosity and permeability.
2. Increasing volumes of clays and quartz have only a minor impact on permeability in these tight carbonate rocks.
3. Increased permeability in these tight carbonate reservoir rocks is associated with good pore connectivity that occurs in rocks with micro-intercrystalline and meso-intragranular pore types. The fluid flow is controlled by pore-throat sizes greater than 0.1 µm.

4. Nano-intercrystalline pore systems represent the most common pore system in the Kometan Formation. This pore system has permeability which is more sensitive to changes in effective stress than the other 2 types of pore system. Consequently there is a higher production risk associated with reservoirs composed predominantly of this type of pore system as the pore pressures decline during production. The Taq Taq, Kirkuk (Baba dome), and Jambur fields as well as the Kurdistan region licensed blocks would fall into this category. By contrast, the Khabaz and Bai Hassan oil fields are predominantly composed of the 2 other types of pore system, and hence do not share the same production risk.
5. Abundant stylolites within the Kometan limestones in the Kirkuk embayment act as barriers to fluid flow and reduce the permeability of the reservoir rocks throughout the region. Stylolite and calcite cementation not only provides an obstacle for regional oil migration but also reduces reservoir potential.

Acknowledgements

We would like to thank Ministry of higher education of Kurdistan region-Iraq government for their financial support of this study with in HCDP scholarship. We would also like to thanks North oil company – Iraq (Kirkuk) for access to core plugs. This work was carried out in The University of Leeds Petrophysics Laboratory and The Wolfson Multiphase Flow Laboratory.

References

Ahr , W.M. and Hull, H.B. , 1983 . Burial diagenesis and reservoir development in the North Haynesville (Smackover) Field, Louisiana . Trans. Gulf Coast Assoc. Geol. Soc. v.33 , p.1 – 9 .

Al Hinai, A., Rezaee, M.R., Esteban ,L., and Labani, M.M., 2014. Comparisons of pore size distribution: A case from the Western Australian gas shale formations, Journal of Unconventional Oil and Gas Resources. v.8, p.1-13.

Al-Qayim, B., and Rashid, F., 2012.Reservoir characteristics of the albian upper qmachuqa formation carbonates, Taq Taq oil field, Kurdistan, Iraq. Journal of Petroleum Geology, v.35, no.4, p.317-341.

Alsharhan A. and Sadd J.L., 2000. Stylolites in Lower Cretaceous carbonates reservoirs, U.A.E: Society for Sedimentary Geology Special Publication, v. 69, p.185–207.

Amaefule, J.O., Wolfe, K., Walls, J.D., Ajufo, A.O., and Peterson, E., 1986. Laboratory determination of effective in low-quality reservoir rocks by the pulse decay technique. SPE15149.

Anselmetti, F.S., and Eberli, G.P., 1999. The velocity-deviation Log : a tool to predict pore type and permeability trends in carbonate drill holes from sonic and porosity or density Logs, AAPG Bulletin, v.83 ,p.450–466.

Bourbie, T., and Walls, J., 1982. Pulse Decay Permeability: Analytical Solution and Experimental Test. Journal of Society of Petroleum Engineering, p. 719-721.

Brigaud B., Vincent B., Durlet C., Deconinck J.F., Blanc P., and Trouiller A., 2010. Acoustic properties of ancient shallow-marine carbonates: effects of depositional environments and diagenetic processes (Middle Jurassic, Paris Basin, France), J. Sediment. Res., v. 80, p.791–807.

Budd, D.A., 2002.The relative roles of compaction and early cementation in the destruction of permeability in carbonate grainstones: a case study from the Palaeogene of West-Central Florida, USA, Journal of Sedimentary Reservoir, v. 72 ,p. 116–128.

Burgess C.J., and Peter C.K., 1985. Formation, distribution, and prediction of stylolites as permeability barriers in the Thamama Group, Abu Dhabi: Middle East Oil Technical Conference and Exhibition, 11–14 March 1985, Bahrain.

Byrnes, A.P., 1997. Reservoir characteristics of low-permeability sandstones in the Rocky Mountains. The Mountain Geologist, v.34, p.39-51.

Byrnes, A.P., and Keighin, C.W. , 1993. Effect of confining stress on pore throats and capillary pressure measurements, selected sandstone reservoir rock, AAPG annual convention program, April 25-28, New Orleans, p.82.

Chalmers, G.R.L., Ross, D.J.K., and Bustin, R.M. , 2012. Geological controls on matrix permeability of Devonian Gas Shale in the Horn River and Liard basins, northeastern British Columbia, Canada, International Journal of Coal Geology, v.103, p.120-131.

Choquette, P.W., and Pray, L.C., 1970. Geological nomenclature and classification of porosity in sedimentary carbonates. AAPG Bull. v.54, no.2, p.207–250.

Coates, G.R., Xiao, L.Z., and Prammer, M.G., 1999. NMR Logging: Principles and Applications, p.234, Houston, USA, Halliburton Energy Services.

Davis, J.M., Roy, N.D. Mozley, P.S., and Hall, J.S., 2006. The effect of carbonate cementation on permeability heterogeneity in fluvial aquifers: an outcrop analog study, Sedimentary Geology, v.184, p. 267–280.

Dawson W.C., 1988. Stylolite porosity in carbonate reservoirs, American Association of Petroleum Geologists Search and Discovery Article, American Association of Petroleum Geologists Annual Convention, Houston, Texas, 20–23March 1988, Article #91030.

Dicker, A.J., and Smits, R.M., 1988. A practical approach for determining permeability from laboratory pressure-pulse decay measurements. SPE 17578.

Dou, Q., Sun, Y., and Sullivan, C., 2011. Rock-physics-based carbonate pore type characterization and reservoir permeability heterogeneity evaluation, Upper San Andres reservoir, Permian Basin, west Texas, journal of applied Geophysics., v.74 ,p. 8–18.

Dutton S.P., and Willis B.J., 1998. Comparison of outcrop and subsurface sandstone permeability distribution, Lower Cretaceous Fall River Formation, South Dakota and Wyoming: Journal of Sedimentary Research, v. 68, p. 890–900.

Ehrenberg, S.N., and Nadeau, P.H., 2005. Sandstone vs. carbonate petroleum reservoirs: A global perspective on porosity-depth and porosity permeability relationships. AAPG Bulletin, v. 89, no. 4, p 435–445.

Ehrenberg, S.N., 2006. Porosity Destruction in Carbonate Platforms: Journal of Petroleum Geology, v. 29, p. 41-52.

Ferreira, T., and Rasband, W.S., 2012. Image J user guide, IJ1.46r, revised edition.

Finkel E.A., and Wilkinson B.H., 1990. Stylolitization as source of cement in Mississippian Salem Limestone, west-central Indiana: AAPG Bulletin, v. 74, p. 174–186.

Ghabezloo, S., Sulem, J., Guedon , S., Martineau, F., 2008. Effective stress law for the permeability of a limestone. International Journal of Rock Mechanics and Mining Science.

Giesche, H., 2006. Mercury Porosimetry: A general (practical) overview. Particle & particle systems characterization. v.23, p.9-19.

Gingras M.K., MacMillan B., Balcom B.J., 2002. Visualizing the internal physical characteristics of carbonate sediments with magnetic resonance imaging and petrography: Bulletin of Canadian Petroleum Geology, v. 50, p. 363–369.

Glover, P.W.J., and Déry, N., 2010. Streaming potential coupling coefficient of quartz glass bead packs: dependence on grain diameter, pore size, and pore throat radius. Geophysics, v. 75, F225–F241 .

Glover, P.W.J., and Walker, E., 2009. Grain-size to effective pore-size transformation derived from electrokinetic theory. Geophysics, v. 74, E17–E29.

Glover, P.W.J., Gómez, J.B. and Meredith, P.G., 2000. Fracturing in saturated rocks undergoing triaxial deformation using complex electrical conductivity measurements: Experimental study. Earth and Planetary Science Letters, v.183, p. 201-213.

Glover, P.W.J., Gómez, J.B., Meredith, P.G., Hayashi, K., Sammonds, P.R. and Murrell, S.A.F., 1997. Damage of saturated rocks undergoing triaxial deformation using complex electrical conductivity measurements: Experimental results. Physics and Chemistry of the Earth, v.22, p. 57-61.

Glover, P.W.J., Zadjali, I.I. and Frew, K.A., 2006. Permeability prediction from MICP and NMR data using an electrokinetic approach. Geophysics, v.71, p.F49-F60.

Haines T. J., Michie E.A.H, Neilson J.E., Healy D., 2016. Permeability evolution across carbonate hosted normal fault zones, Marine and Petroleum Geology, v. 72, p.62-82.

Haines, T.J., Neilson, J.E., Healy, D., Michie, E.A.H., and Aplin, A.C., 2015. The impact of carbonate texture on the quantification of total porosity by image analysis, Computers and Geoscience, v.85, p. 112–125.

Harris P.M., 2010. Delineating and quantifying depositional facies patterns in carbonate reservoirs: Insight from modern analogs, AAPG Bulletin, v.94, no. 1 , p. 61–86.

Harris N.B., 2006. Low-porosity haloes at stylolites in the feldspathic Upper Jurassic Ula sandstone, Norwegian North Sea: An integrated petrographic and chemical mass-balance approach: Journal of Sedimentary Research, v. 76, p.444–459.

Heap, M.J., Baud P., Reuschlé T., and Meredith P. G.,2014 , Stylolites in limestones: Barriers to fluid flow, Geology , v.42, no.1 , p.51-54.

Heath, J.E., Dewers T.A., McPherson B.J.O.L., Petrusak R., Chidsey T.C., Rinehart A.J., and Mozley P.S., 2011. Pore networks in continental and marine mudstones: characteristics and controls on sealing behaviour, Geosphere, v. 7 , p. 429–454.

Hollis, C., Vahrenkamp, V., Tull, S., Mookerjee, A., Taberner, C., Huang, Y., 2010. Pore system characterisation in heterogeneous carbonates: An alternative approach to w idely-used rock-typing methodologies. Marine and Petroleum Geology. v.27, no. 4, p. 772-793.

Jannot, Y., Lasseux, D., Vizé, G., and Hamon, G., 2007. A detailed analysis of permeability and Klinkenberg coefficient estimation from unsteady-state pulse-decay or draw-down experiments. Paper no. SCA2007-08.

Jones, S.C.,1997. A Technique for Faster Pulse-Decay Permeability Measurements in Tight Rocks.

Katz, A.J. and Thompson, A.H., 1986. Quantitative prediction of permeability in porous rock. Physical Review B, v.34, p.8179-8181.

Koepnick R.B., 1987, Distribution and permeability of stylolite-bearing horizons within a Lower Cretaceous carbonate reservoir in the Middle East:Society of Petroleum Engineers Formation Evaluation, v. 2.

Loucks, R.G. , 2002.Controls on reservoir quality in platform-interior limestones around the Gulf of Mexico : example from the lower Cretaceous Pearsall formation in South Texas depositional setting and systems of the Pearsall formation, Gulf Coast Assoc. Geol. Soc. Trans., v.52 , p. 659–672.

Lucia, F.J., 1995, Rock-fabric/petrophysical classification of carbonate pore Space for reservoir characterization, AAPG Bulletin., v.79, p. 1275–1300.

Lucia, F.J., 2007 .Carbonate Reservoir Characterization: an Integrated Approach, (second edition) Springer (2007).

Makhloufi Y. , Collin P., Bergerata F., Casteleync, L. , Claesd, S., David, C., Menendezc B., Monnae F., Robionc P. , Sizunf J., Swennend R., and Rigolletg C., 2013 . Impact of sedimentology and diagenesis on the petrophysical properties of a tight oolitic carbonate reservoir. The case of the Oolithe Blanche Formation (Bathonian, Paris Basin, France), Marine and Petroleum Geology, v. 48, p.323–340.

Melim L.A., Anselmetti F.S., and Eberli G.P., 2001. The importance of pore type on permeability of Neogene carbonates, Great Bahama Bank Subsurface Geology of a Prograding Carbonate Platform Margin Great Bahama Bank Results of the Bahamas Drilling Project, SEPM Special Publication, p. 217–238.

Moore, C.H. and Druckman , Y. , 1981 . Burial diagenesis and porosity evolution, Upper Jurassic Smackover, Arkansas and Louisiana. AAPG Bulletin, v. 65, p. 597 – 628.

Nelson R.A., 1981. Significance of fracture sets associated with stylolite zones: The American Association of Petroleum Geologists Bulletin, v. 65, p. 2417–2425.

North Oil Company ,1987. Final well repot , Taq Taq oil field.

Palermo, D., Aigner, T., Nardon, S., and Blendinger, W.,2010. Three-dimensional facies modeling of carbonate sand bodies: outcrop analog study in an epicontinental basin (Triassic, southwest Germany), AAPG Bulletin, v.94 , p. 475–512.

Porras, J., and Campos, O., 2001. Rock Typing: A Key Approach for Petrophysical Characterization and Definition of Flow Units, Santa Barbara Field, Eastern Venezuela Basin, SPE 69458, SPE Latin American Conference, Buenos Aires, Argentina..

Rashid, F., Glover, P.W.J., Lorinczi, P., Hussein, D., Collier, R, 2015b. Permeability prediction in tight carbonate rocks using capillary pressure measurements, marine and petroleum geology, v.68 Part A, p.536-550.

Rashid, F., Glover, P.W.J., Lorinczi, P., Collier, R., and Lawrence, J., 2015a. Porosity and permeability of tight carbonate reservoir rocks in the north of Iraq. Journal of Petroleum Science and Engineering, v.133, p.147-161.

Raynaud, S., and Carrio-Schaffhauser E., 1992. Rock matrix structures in a zone influenced by a stylolite: Journal of Structural Geology, v.14, p.973–980.

Rezaee, M.-R., Motiei , H., and Kazemzadeh, E., 2007. A new method to acquire *m* exponent and tortuosity factor for microscopically heterogeneous carbonates, Journal of Petroleum Science and Engineering, v. 56, p. 241–251.

Ronchi P., Giulio A. Di, Ceriani A., and Scotti P., 2010. Contrasting fluid events giving rise to apparently similar diagenetic products; late-stage dolomite cements from the Southern Alps and central Apennines, Italy, Geological Society of London, Special Publications, v. 329, p. 397–413.

Rong, H., Jiao, Y., Wu ,L., Gu, Y., Zhang, L., Li ,R., and Zeng ,F.,2012. Effects of diagenesis on the acoustic velocity of the Triassic oolitic shoals in the Yudongzi outcrop of Erlangmiao area, Northwest Sichuan Basin, Journal of Earth Science, v.23, p. 542–558.

Schmoker, J. W. and Halley, R. B. , 1982. Carbonate porosity versus depth; a predictable relation for South Florida. AAPG Bulletin., v.66, p.2561 – 2570.

Sella, G.F., Dixon, T.H. and Mao, A., 2002. REVEL: A model for recent plate velocities from space geodesy. Journal of Geophysical Research, v. 107, no. B4, 2081, p. 30.

Swanson, B. F., 1981, A simple correlation between permeabilities and mercury capillary pressures: Journal of Petroleum Technology, v.33, p.2498– 2504.

Van Baaren, J.P., 1979, Quick-look permeability estimates using sidewall samples and porosity logs: Transactions of the 6th Annual European Logging Symposium, Society of Petrophysicists and Well Log Analysts, p.19–25.

Van der Land, C., Wood, R., Wu, K., van Dijke, M.I.J., Jiang, Z., Corbett, P.W.M., and Couples, G., 2013. Modelling the permeability evolution of carbonate rocks, marine and petroleum geology, v. 48, p. 1–7.

Van Geet, M., Swennen R., and Wevers M., 2001. Towards 3-D petrography: Application of microfocus computer tomography in geological science: Computers and Geosciences, v. 27, p. 1091–1099.

Washburn, E. W., 1921. The Dynamics of Capillary Flow. Physical Review, v.17, p.273-283.

Webb, P. A., 2001. An Introduction to the physical characterization of materials by mercury intrusion porosimetry with emphasis on reduction and presentation of experimental data. Norcross, Georgia.

Weger, R.J., Eberli G.P., Baechle G.T., Massaferro J.L., and Sun Y.-F., 2009. Quantification of pore structure and its effect on sonic velocity and permeability in carbonates, AAPG Bulletin., v.93, p. 1297–1317

Westphal, H., Eberli, G.P., Smith, L.B., Grammer, G.M., and Kislak, J., 2004. Reservoir characterization of the Mississippian Madison Formation, Wind River basin, Wyoming, AAPG Bulletin, v. 88, p. 405–432.

Westphal, H., Surholt, I., Kiesl, C., Thern, H.F. and Kruspe, T., 2005. NMR Measurements in Carbonate Rocks: Problems and an Approach to a Solution. Pure and Applied Geophysics, v.162, p.549-570.

Wilson, M.E.J. and Evans, M.J., 2002. Sedimentology and diagenesis of Tertiary carbonates on the Mangkalihat Peninsula, Borneo: implications for subsurface reservoir quality. Marine and petroleum geology, v.19,p.873-900.

Zebari, M., 2013 .Geometry and Evolution of Fold Structures within the High Folded Zone: Zagros Fold-Thrust Belt, Kurdistan region-Iraq, published MSc thesis, University of Nebraska.

Zebari, M., and Burberry, C.M., 2015. 4-D evolution of anticlines and implications for hydrocarbon exploration within the Zagros Fold-Thrust Belt, Kurdistan Region, Iraq. GeoArabia; Gulf PetroLink, Bahrain, v.20, p.161-188.

Zhang, M., Takahashi, M., Morin, R. H. and Esaki, T., 2000. Evaluation and Application of the Transient-Pulse Technique for Determining the Hydraulic Properties of Low-Permeability Rocks – Part 1: Theoretical Evaluation. American Society for Testing and Materials : Geotechnical Testing Journal, p.83-90.

Zhao, H., Ning, Z., Zhao, T., Zhang, R., Wang, Q., 2016. Effects of mineralogy on petrophysical properties and permeability estimation of the Upper Triassic Yanchang tight oil sandstones in Ordos Basin, Northern China, Fuel, v. 186, p. 328-338.

Figures titles

Figure 1. Physiographic map of the Zagros showing main subdivisions segments of the belt, and highlights oil fields and wells used in this study (Core sampling and testing strategy after Sella et al., 2002; Zebari M., 2013; Zebari M. M. and Burberry C. M. 2015).

Figure 2. Two typical sedimentary logs of the Kometan Formation throughout the study area calibrated with the gamma ray deflection. The rock textures are classified as Globigerinal wackstone/packstone limestone (GWP), globigerinal and oligosteginal wackstone/packstone textures (GOWP) and globigerinal mudstone (GM). (A) Well representing the Bai Hassan field, (B) well representing the Taq Taq field.

Figure 3. Pore system types were investigated throughout the studied samples. Nano intercrystalline pore system; A1: SEM micrography shows intercrystalline pores size smaller than 1 µm, A2: Pore size distribution obtained from image analysis, A3: NMR T2 spectra < 100 ms, A4: MICP pore throat size distribution < 0.1 µm. Micro intercrystalline pore system; B1: SEM micrography shows intercrystalline pores size larger than 1 µm, B2: Pore size distribution achieved from image analysis , B3: NMR T2 spectra > 100 ms, B4: MICP pore throat size distribution < 0.2 µm. Meso intragranular and moldic pore system; C1: SEM micrography shows intragranular and moldic pores size larger than 10 µm, C2: Pore size distribution measured from image analysis, C3: NMR T2 spectra > 200 ms, C4: MICP pore throat size distribution < 0.2 µm.

Figure 4. The relationship between porosity (helium) and permeability (helium, Klinkenberg-corrected) for the samples measured in the Kometan Formation. A: Photomicrograph of polarizing microscope thin section images impregnated with blue epoxy. The traces of blue hue in intercrystalline pores show it has a mudstone texture with a porosity of 0.1876 and a permeability of 0.50 mD. B: Photomicrograph of polarizing microscope thin section images impregnated with blue epoxy, does not show any traces of blue hue pores, it has a wackstone texture with a porosity of 0.032 and a permeability of 0.018 mD permeability.

Figure 5. Measured vertical helium permeability as a function of the measured horizontal helium permeability (both klinkenberg-corrected) for 16 selected samples from the available core data.

Figure 6. The effect of confining pressure (effective, psi) on the magnitude of permeability for two samples for each of the three recognized pore types:

The Nano-intercrystalline pore system: A1: SEM micrography shows intercrystalline pores size smaller than 1 µm, A2: Photomicrograph of polarizing microscope thin section image shows wackstone texture. A3 Samples 1 and 2: Permeability variation of these samples as function of effective stress.

The Micro-intercrystalline pore system; B1: SEM micrography shows intercrystalline pores size greater than 1 µm, B2: Photomicrograph of polarizing microscope thin section image shows mudstone texture. B3 samples 3 and 4: Permeability variation of these two samples as function of effective stress.

The Meso-intragranular pore system; C1: SEM micrography shows intragranular pores size greater than 10 µm, C2: Photomicrograph of polarizing microscope thin section image shows wackstone texture contains blue traced intragranular pores. C3 samples 5 and 6: Permeability variation of selected samples as function of effective stress.

Figure 7. Log–log plot of Klinkenberg-corrected helium permeability as a function of helium porosity for a subset of 24 samples measured in this study (measured under at ambient conditions). The dashed lines correspond to power law fits through the stylolitic (red line, red symbols) and the non-stylolitic samples (green line, green symbols). Two highlighted samples represent mudstone rock texture for both stylolitic and non-stylolitic samples.

Figure 8. Effects of mineralogy on permeability in tight carbonate rocks; A1: Klinkenberg-corrected Permeability as a function of Illite-smectite % volume, and A2: brine permeability as a function of Illite-smectite % volume. B1: Klinkenberg-corrected permeability as a function of quartz % volume, B2: Brine permeability as a function of quartz % volume.

Figure 9. Measured klinkenberg-corrected permeability as a function of pore diameter for the 3 recognised pore types: including nano-intercrystalline, micro-intercrystalline and meso-intercrystalline pore systems.

Figure 10. Measured klinkenberg-corrected permeability as a function of the pore throat size for 21 samples. The pore throat size has been calculated from the application of the Washburn equation to the measured at threshold point on the respective capillary pressure curve.

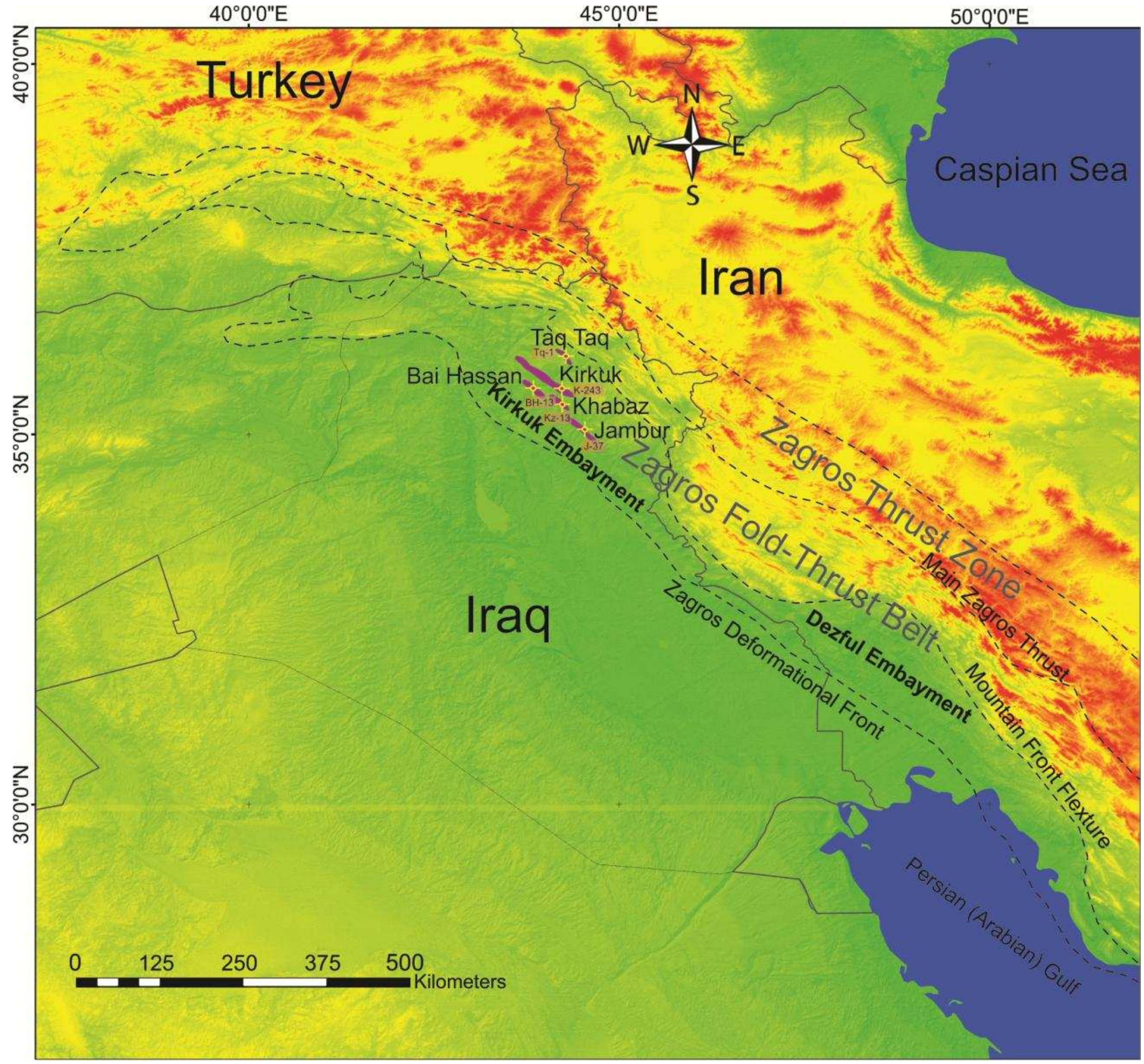
40°0'0"E
45°0'0"E
50°0'0"E
40°0'0"N
35°0'0"N
30°0'0"N
Turkey
N
W
E
S
Caspian Sea
Iran
Taq Taq
Tq-1
Bai Hassan
Kirkuk
K-243
BH-13
Khabaz
Kz-13
Jambur
J-37
Kirkuk Embayment
Zagros Thrust Zone
Zagros Fold-Thrust Belt
Main Zagros Thrust
Iraq
Zagros Deformational Front
Dezful Embayment
Mountain Front Flexture
Persian (Arabian) Gulf
0
125
250
375
500
Kilometers

Figure 1

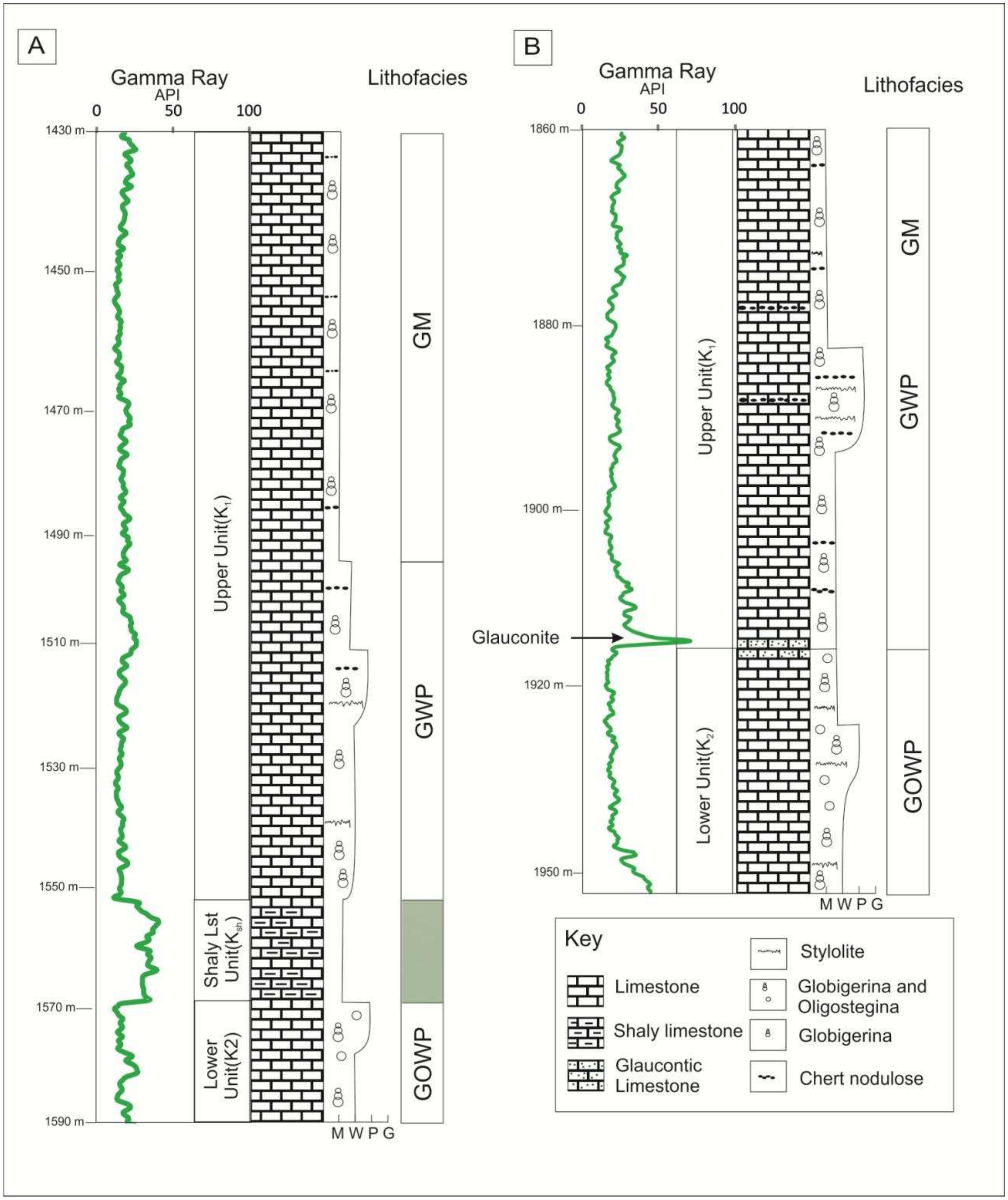

A
Gamma Ray
API
0
50
100
Lithofacies
1430 m
1450 m
1470 m
1490 m
1510 m
1530 m
1550 m
1570 m
1590 m
Upper Unit(K1)
Shaly Lst Unit(Ksh)
Lower Unit(K2)
GM
GWP
GOWP
M W P G
B
Gamma Ray
API
0
50
100
Lithofacies
1860 m
1880 m
1900 m
1920 m
1950 m
Glauconite
Upper Unit(K1)
Lower Unit(K2)
GM
GWP
GOWP
M W P G
Key
Limestone
Shaly limestone
Glauocontic Limestone
Stylolite
Globigerina and Oligostegina
Globigerina
Chert nodulose

Figure 2

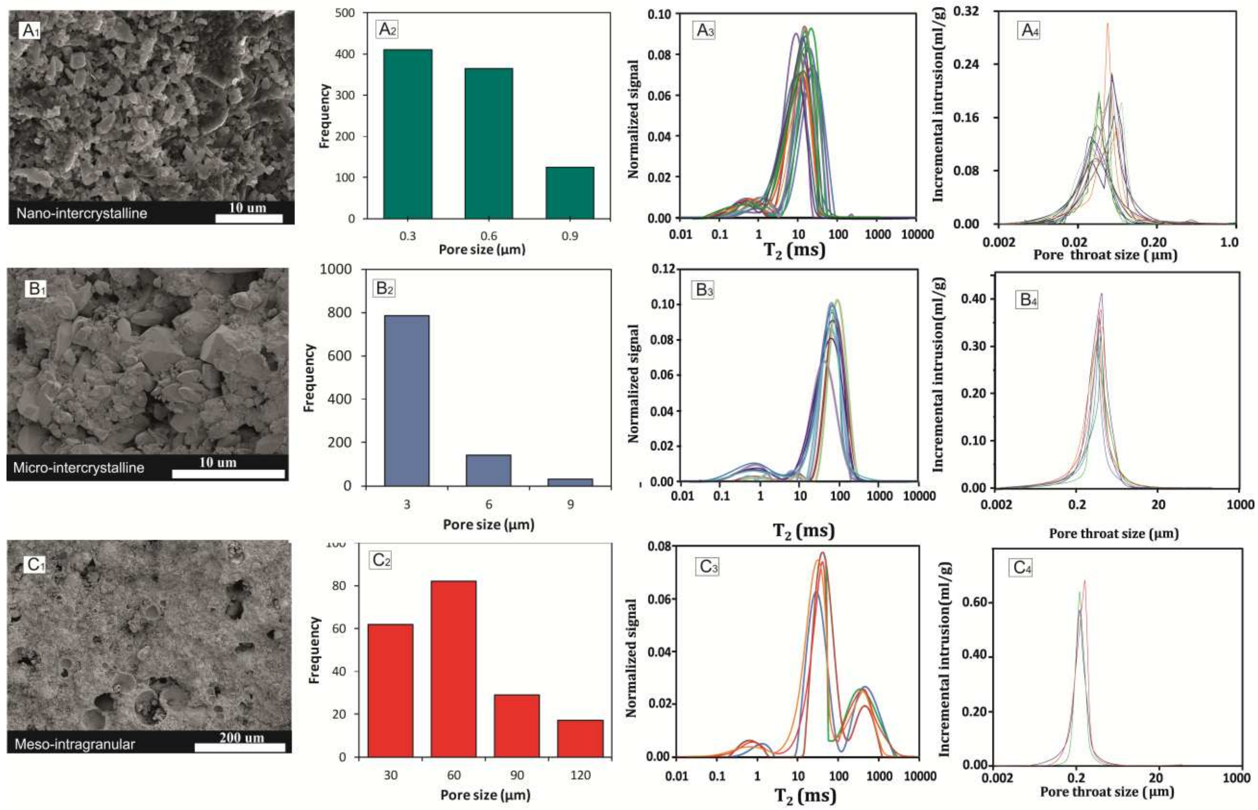
A1
Nano-intercrystalline
10 um
A2
Frequency
Pore size (μm)
A3
Normalized signal
T2 (ms)
A4
Incremental intrusion(ml/g)
Pore throat size (μm)
B1
Micro-intercrystalline
10 um
B2
Frequency
Pore size (μm)
B3
Normalized signal
T2 (ms)
B4
Incremental intrusion(ml/g)
Pore throat size (μm)
C1
Meso-intragranular
200 um
C2
Frequency
Pore size (μm)
C3
Normalized signal
T2 (ms)
C4
Incremental intrusion(ml/g)
Pore throat size (μm)

Figure 3

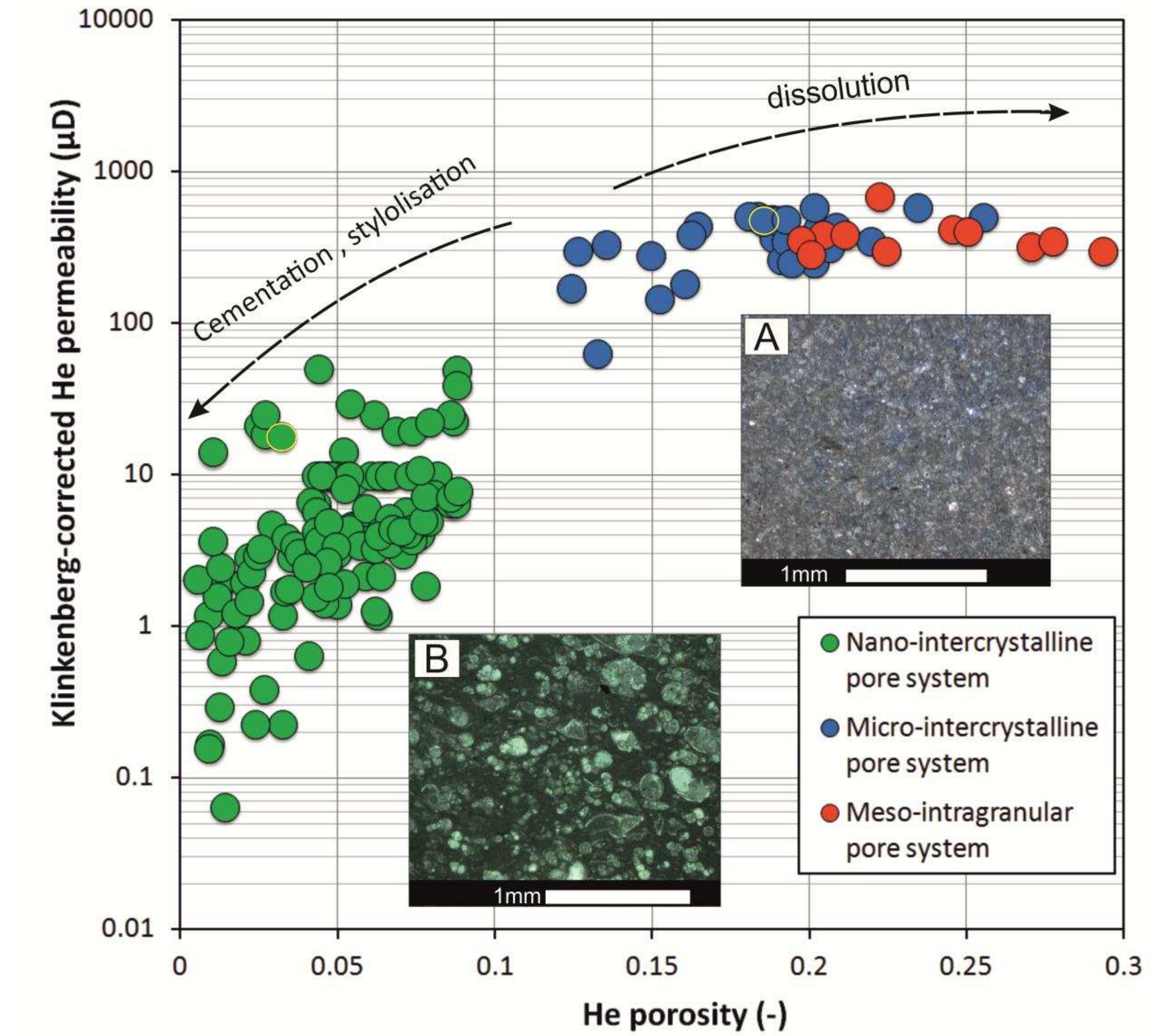
dissolution
Cementation , stylolisation
A
1mm
B
1mm
Nano-intercrystalline pore system
Micro-intercrystalline pore system
Meso-intragranular pore system
Klinkenberg-corrected He permeability (µD)
10000
1000
100
10
1
0.1
0.01
0
0.05
0.1
0.15
0.2
0.25
0.3
He porosity (-)

Figure 4

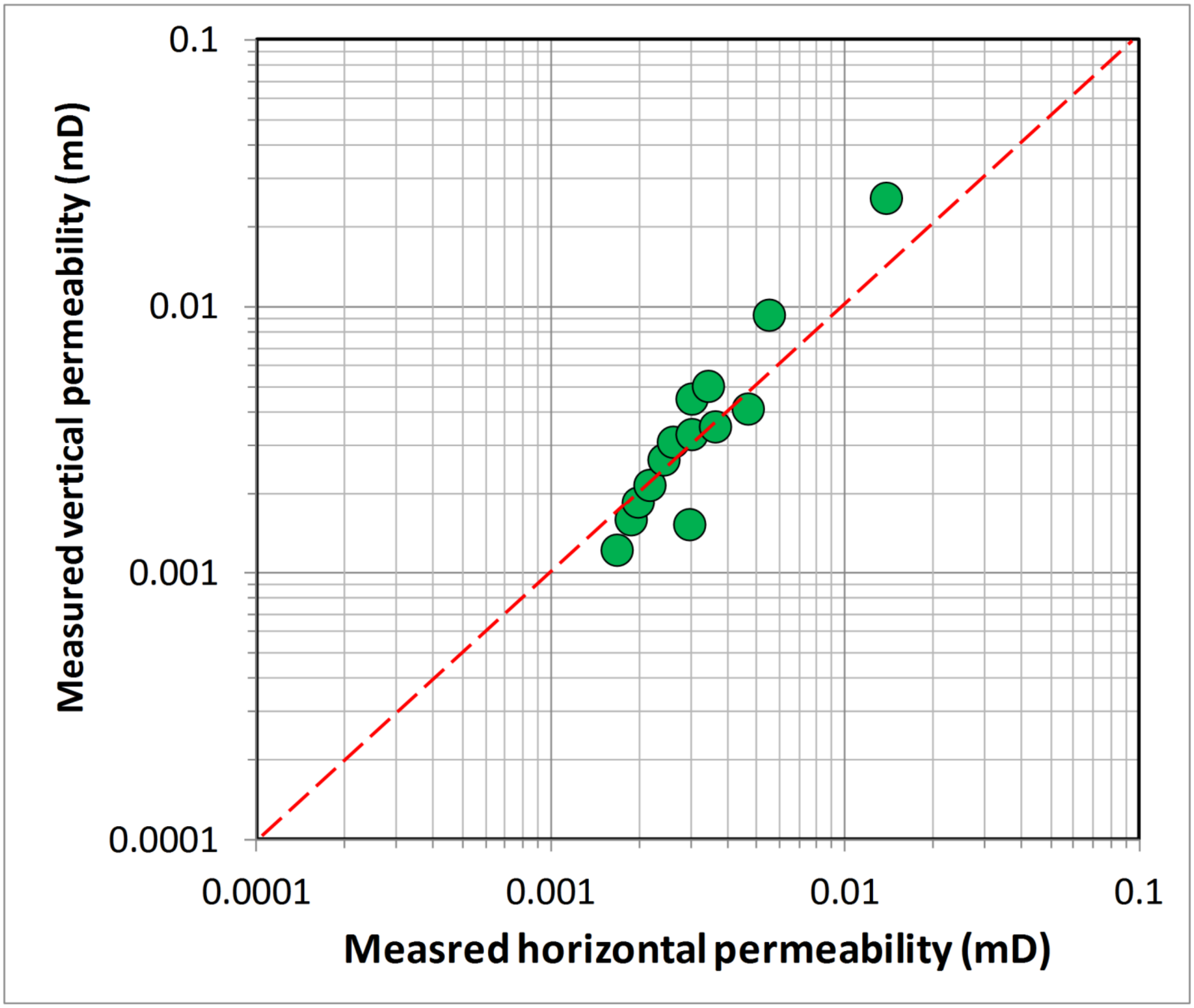
0.1
0.01
0.001
0.0001
Measured vertical permeability (mD)
0.0001
0.001
0.01
0.1
Measred horizontal permeability (mD)

Figure 5

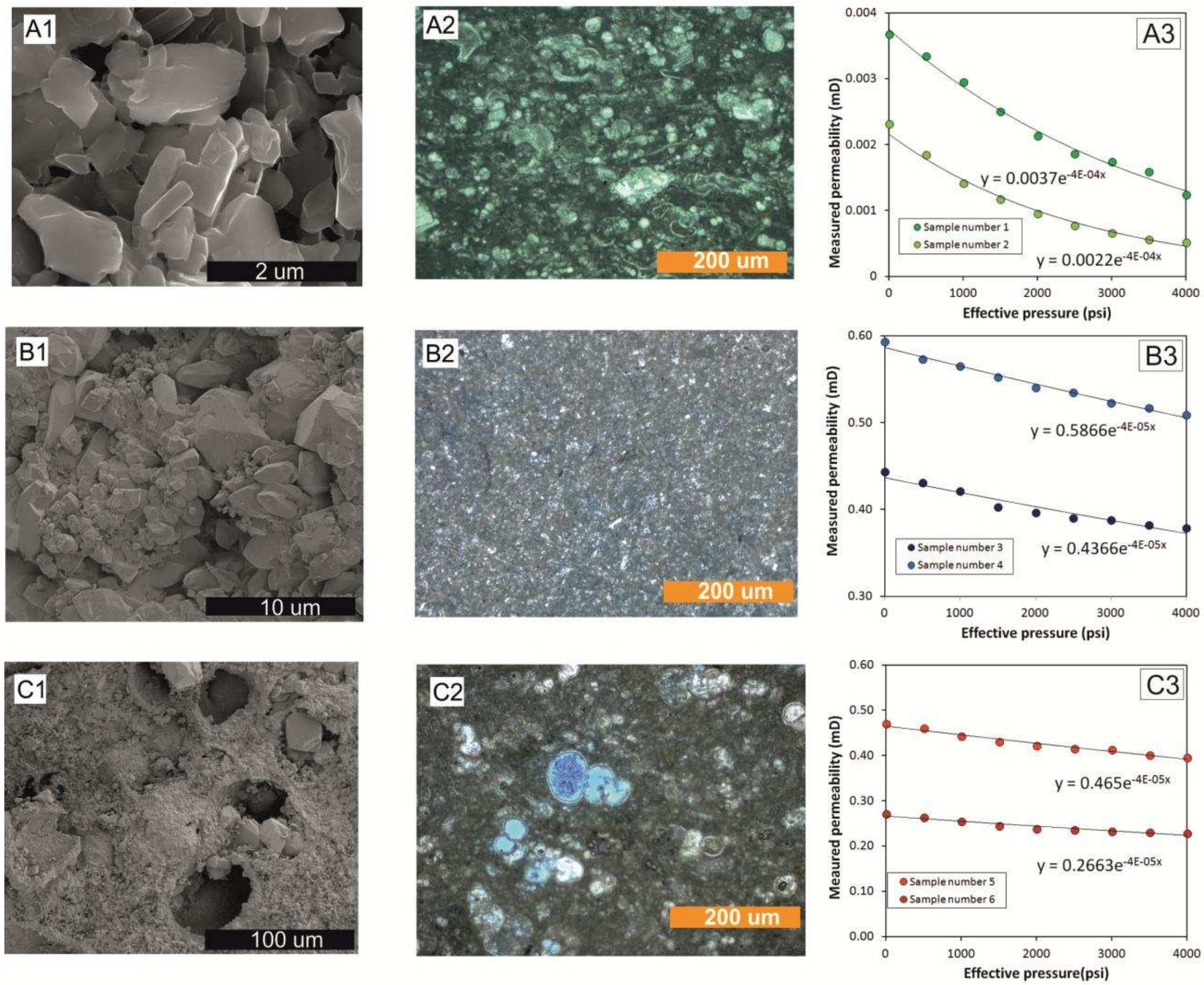
A1
2 um
A2
200 um
A3
0.004
0.003
0.002
0.001
0
Measured permeability (mD)
y = 0.0037e^-4E-04x
y = 0.0022e^-4E-04x
Sample number 1
Sample number 2
0
1000
2000
3000
4000
Effective pressure (psi)
B1
10 um
B2
200 um
B3
0.60
0.50
0.40
0.30
Measured permeability (mD)
y = 0.5866e^-4E-05x
y = 0.4366e^-4E-05x
Sample number 3
Sample number 4
0
1000
2000
3000
4000
Effective pressure (psi)
C1
100 um
C2
200 um
C3
0.60
0.50
0.40
0.30
0.20
0.10
0.00
Meaured permeability (mD)
y = 0.465e^-4E-05x
y = 0.2663e^-4E-05x
Sample number 5
Sample number 6
0
1000
2000
3000
4000
Effective pressure(psi)

Figure 6

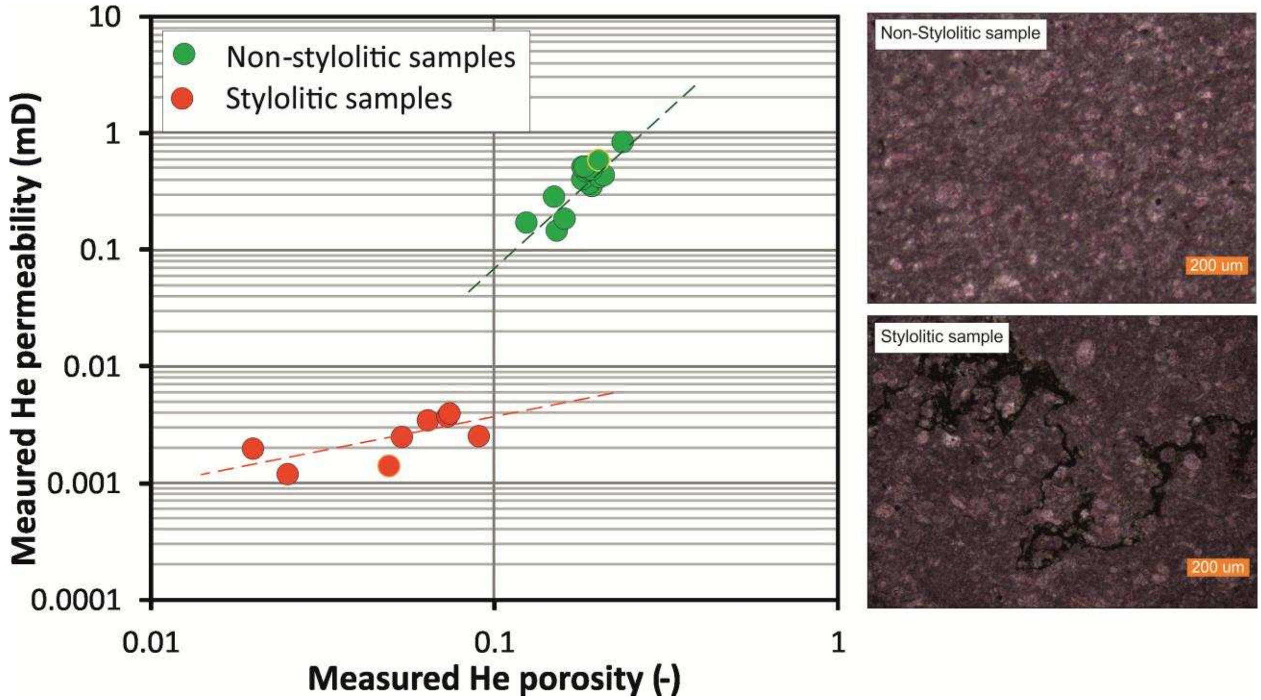
Non-stylolitic samples
Stylolitic samples
Meaured He permeability (mD)
10
1
0.1
0.01
0.001
0.0001
0.01
0.1
1
Measured He porosity (-)
Non-Stylolitic sample
200 um
Stylolitic sample
200 um

Figure 7

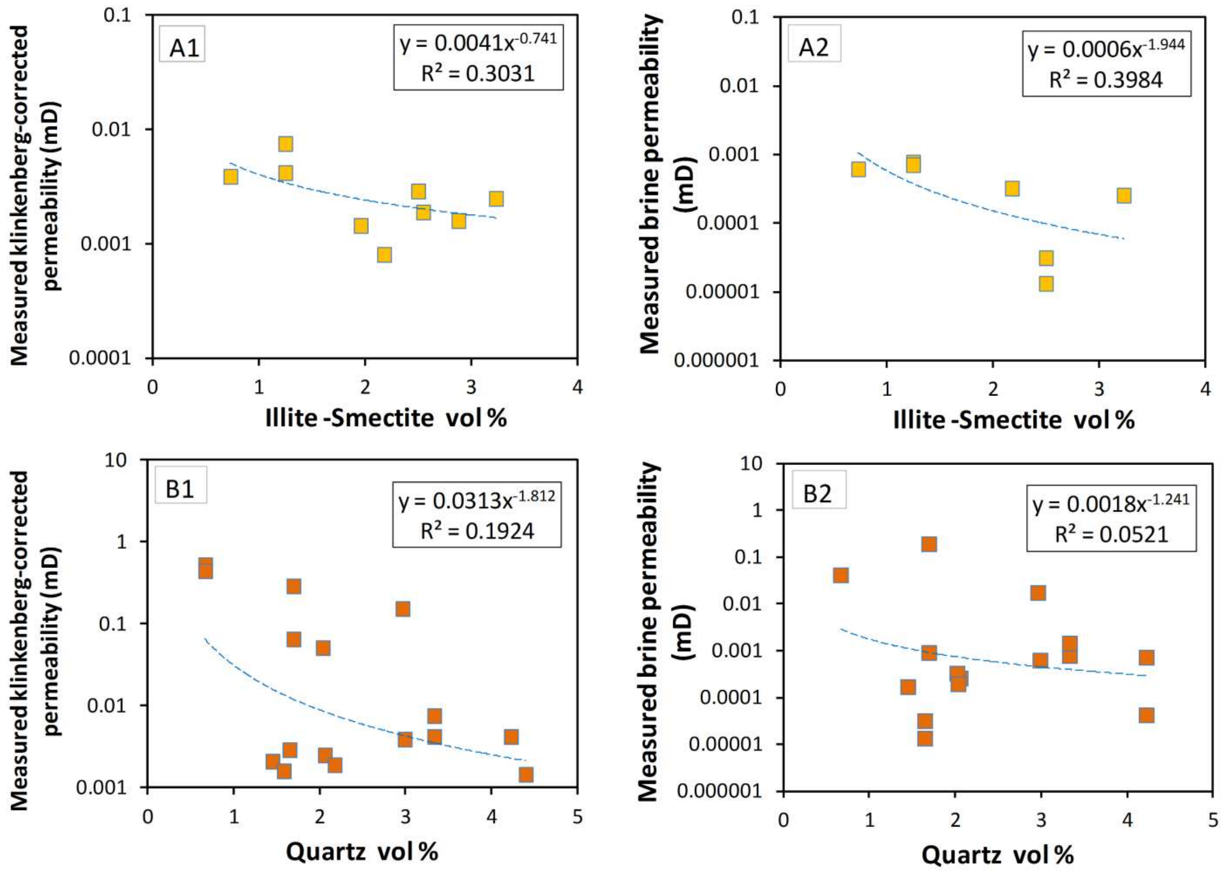
A1
y = 0.0041x-0.741
R² = 0.3031
Measured klinkenberg-corrected permeability (mD)
Illite -Smectite vol %
A2
y = 0.0006x-1.944
R² = 0.3984
Measured brine permeability (mD)
Illite -Smectite vol %
B1
y = 0.0313x-1.812
R² = 0.1924
Measured klinkenberg-corrected permeability (mD)
Quartz vol %
B2
y = 0.0018x-1.241
R² = 0.0521
Measured brine permeability (mD)
Quartz vol %

Figure 8

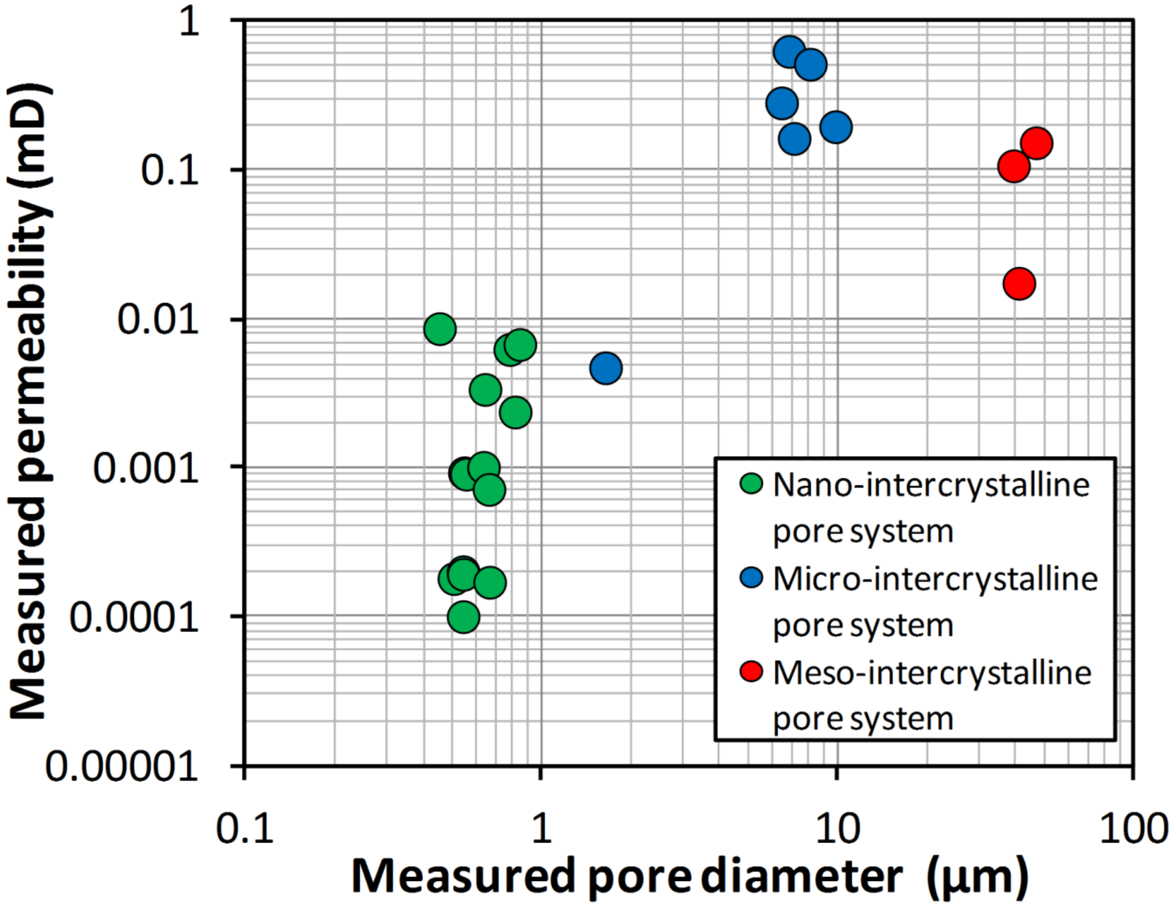

1
0.1
0.01
0.001
0.0001
0.00001
Measured permeability (mD)
0.1
1
10
100
Measured pore diameter (μm)
Nano-intercrystalline pore system
Micro-intercrystalline pore system
Meso-intercrystalline pore system

Figure 9

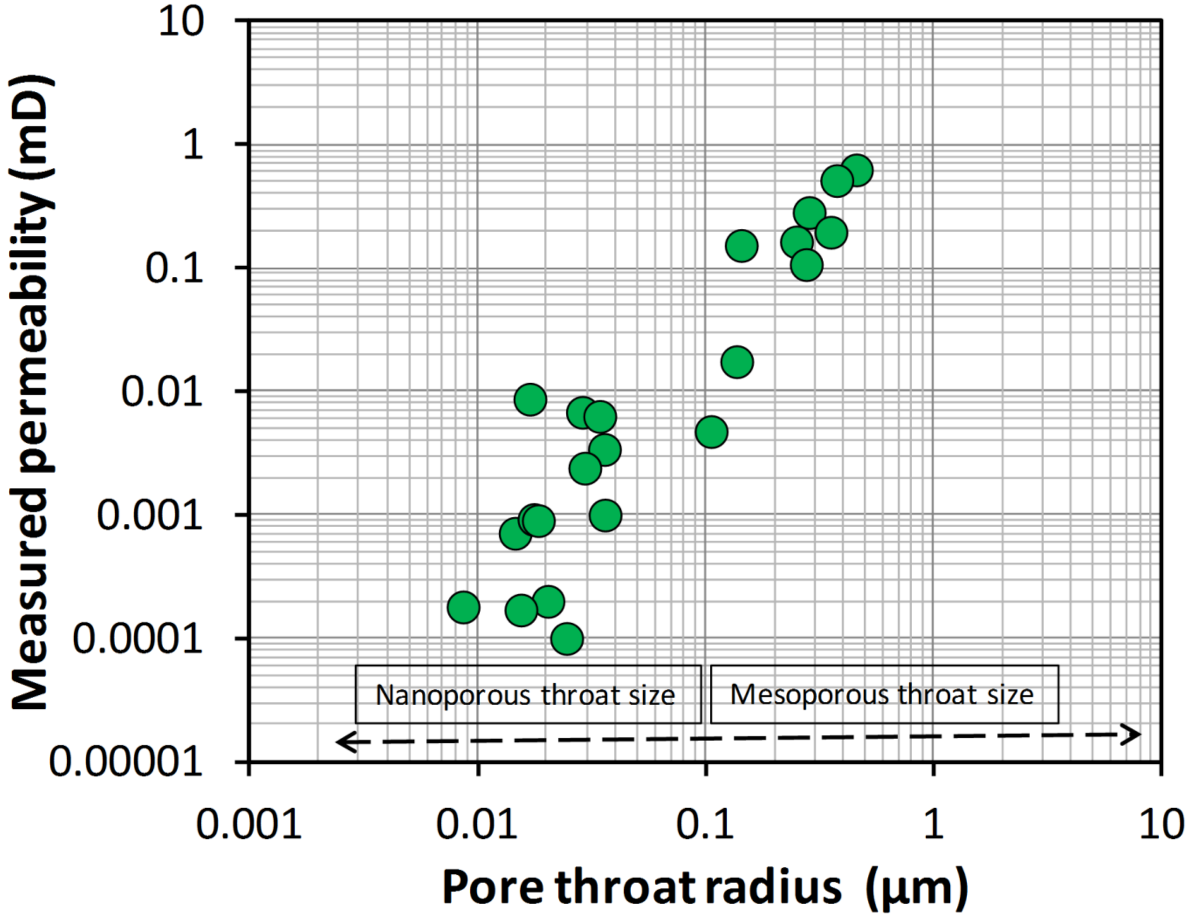
10
1
0.1
0.01
0.001
0.0001
0.00001
Measured permeability (mD)
Nanoporous throat size
Mesoporous throat size
0.001
0.01
0.1
1
10
Pore throat radius (µm)

1 Figure 10